J Fluoresc (2008) 18:1029–1034
DOI 10.1007/s10895-008-0327-0

ORIGINAL PAPER

Defect Structure and Up-conversion Luminescence Properties of ZrO_2:Yb^{3+},Er^{3+} Nanomaterials

Iko Hyppänen · Jorma Hölsä · Jouko Kankare · Mika Lastusaari · Laura Pihlgren · Tero Soukka

Received: 31 October 2007 / Accepted: 22 January 2008 / Published online: 8 February 2008

Abstract The up-converting ZrO_2:Yb^{3+},Er^{3+} nanomaterials were prepared with the combustion and sol–gel methods. FT-IR spectroscopy was used for analyzing the impurities. The crystal structures were characterized with X-ray powder diffraction and the mean crystallite sizes were estimated with the Scherrer formula. Up-conversion luminescence measurements were made at room temperature with IR-laser excitation at 977 nm. The IR spectra revealed the conventional NO_3^- and OH^- impurities for the combustion synthesis products. The structure of the ZrO_2:Yb^{3+}, Er^{3+} nanomaterials was cubic except for the minor monoclinic and tetragonal impurities obtained with the sol–gel method. The materials showed red (650–700 nm) and green (520–560 nm) up-conversion luminescence due to the $^4F_{9/2}\rightarrow{}^4I_{15/2}$ and ($^2H_{11/2}$, $^4S_{3/2}$)$\rightarrow{}^4I_{15/2}$ transitions of Er^{3+}, respectively. The products obtained with the combustion synthesis exhibited the most intense luminescence intensity and showed considerable afterglow.

Keywords Zirconium oxide · Nanocrystals · Combustion · Sol–gel · Up-conversion luminescence

I. Hyppänen · J. Hölsä · J. Kankare · M. Lastusaari · L. Pihlgren (✉)
Department of Chemistry, University of Turku,
FI-20014 Turku, Finland
e-mail: laerle@utu.fi

L. Pihlgren · T. Soukka
Department of Biotechnology, University of Turku,
Tykistökatu 6,
FI-20520 Turku, Finland

L. Pihlgren
Graduate School of Materials Research,
Turku, Finland

Introduction

Since the discovery of the up-conversion phenomena [1], there has been an ever increasing interest in up-converting phosphors in which the absorption of two or more low energy photons is followed by emission of a higher energy photon. Most up-conversion luminescence materials operate by using a combination of a trivalent rare earth (lanthanide) sensitizer (*e.g.* Yb, Er or Sm) and an activator (*e.g.* Er, Ho, Pr or Tm) ion in a crystal lattice [2, 3]. Up-converting phosphors have a variety of potential applications as lasers and displays as well as inks for security printing (*e.g.* bank notes and bonds) [4–6]. One of the most sophisticated applications of lanthanide up-conversion luminescence is probably in medical diagnostics [7]. However, there are some major problems in the use of photoluminescence based on the *direct* UV excitation in immunoassays [8]. Human blood absorbs strongly UV radiation as well as the emission of the phosphor in the visible [9]. A promising way to overcome the problems arising from the blood absorption is to use a long wavelength excitation and benefit from the up-conversion luminescence [10]. Since there is practically no absorption by the whole-blood in the near IR region it has no capability for up-conversion in the excitation wavelength region of the conventional up-converting phosphors based on the Yb^{3+} (sensitizer) and Er^{3+} (activator) combination.

In order to accomplish an efficient coupling to biological compounds, nanosized material particles are needed. Nanomaterials with high up-conversion luminescence efficiency are also required in the development of novel homogeneous label technology for quantitative all-in-one whole-blood immunoassay which uses low-cost measurement devices [11].

In addition to the local environment, the dopant concentration, as well as the distribution of active ions in

the host material, the properties of the host lattice affect the up-conversion efficiency [12]. Zirconia offers an ideal medium for the preparation of highly luminescent materials because of its chemical and photochemical stability, high refractive index (2.15–2.18) and low phonon energy. The stretching frequency of the Zr-O –bond is about 470 cm^{-1}, which is much lower than for Al–O (870) or Si–O (1100) though higher than for Y–O (300–380 cm^{-1}) [12].

In addition, due to the different charge compensation effects in the ZrO_2 host, the lanthanide dopants possess a multisite position that should improve the absorption efficiency and potentially make the energy transfer from the sensitizer (Yb^{3+}) to the activator (Er^{3+}) more efficient.

In this work, nanocrystalline up-converting ZrO_2:Yb^{3+},Er^{3+} materials were prepared with selected soft chemistry methods known to yield nanosized products, *e.g.* combustion and sol–gel methods. The impurities of the products were studied with FT-IR spectroscopy while the crystal structure and phase purities were analyzed with X-ray powder diffraction (XPD). Up-conversion luminescence was obtained at room temperature with near infrared (NIR) excitation. The up-conversion luminescence intensity was found to depend on the crystallite size, the crystal structure as well as the impurities of the materials. The reasons behind this behavior are presented and discussed.

Experimental

The method of synthesis affects not only the type and amount of impurities but has also an effect on the crystallite size, which in turn has a strong influence on the intensity of conventional luminescence. The combustion synthesis is a rapid method with high synthesis temperature to produce nanomaterials. The sol–gel method is a much slower method but produces pure nanomaterials with much less organic impurities. The slow reaction rate may affect, however, the uniform and homogeneous substitution of the tetravalent Zr^{IV} ions with the trivalent Yb^{3+} and Er^{3+} ions, as discussed later.

The nanocrystalline ZrO_2:Yb^{3+},Er^{3+} materials—where the nominal mole fractions *vis-à-vis* zirconium were 0.10 and 0.04 for ytterbium and erbium, respectively—were prepared with the combustion [13] and sol–gel methods [14] using $ZrO(NO_3)_2{\cdot}5H_2O$ (99.99%, Aldrich), Yb_2O_3 (3N, Rhône-Poulenc) and Er_2O_3 (4N, Aldrich) as precursor chemicals. In the combustion synthesis, the aqueous solutions of zirconyl nitrate and ytterbium and erbium nitrates were used rather than the original solid compounds. Glycine (NH_2CH_2COOH), semicarbazide ($H_2NCONHNH_2{\cdot}HCl$), urea ($(NH_2)_2CO$), citric acid ($HOC(COOH)(CH_2COOH)_2$) or 2-amino-2-methyl-1,3-propanediol (AMP, $(HOCH_2)_2C(NH_2)CH_3$) served as the fuel. Ammonium nitrate (NH_4NO_3) was used as an oxidizer. The combustion reaction was carried out in a glass reactor using a weak upward air flow. Selected products were post-annealed in air at 700 °C for 1 h.

The ZrO_2:Yb^{3+},Er^{3+} nanomaterials obtained with the sol–gel method utilized the zirconium-*n*-propoxide as a precursor to which the aqueous ytterbium and erbium nitrates were added. After gelation for 2 h the materials were dried (24 h) and annealed for 3 or 6 h at 400 °C and 10 or 20 h at 1000 °C in static air in a ceramic crucible with a lid.

The FT-IR spectra between 400 and 4000 cm^{-1} were measured with a Mattson Instruments GALAXY 6030 spectrometer with a 4 cm^{-1} resolution. The materials were mixed with KBr (Spectranal, Riedel-de Haën) and then pressed to transparent discs.

The crystal structure and phase purity of the ZrO_2:Yb^{3+},Er^{3+} nanomaterials were analyzed with the X-ray powder diffraction (XPD) measurements. The patterns were collected with a Huber 670 image plate (2θ range: 4–100°, step: 0.005°) Guinier-camera ($CuK\alpha_1$ radiation, λ=1.5406 Å).

The average crystallite size of each ZrO_2:Yb^{3+},Er^{3+} nanomaterial was estimated from the diffraction data by using the Scherrer formula (Eq. 1) [15] where D is the average crystallite size (m), λ the X-ray wavelength (m), β the full width at half maximum (FWHM) of the selected reflection (rad) and θ (°) half of the Bragg's angle (2θ). The reflection broadening due to the diffractometer was eliminated from the β_s-value by using a microcrystalline ZrO_2 reference (β_r) (Eq. 2). In the present work, the [111] reflection (2θ=30.2°) was used in the calculations.

$$D = \frac{0.9 \times \lambda}{\beta \times \cos\theta} \tag{1}$$

$$\beta^2 = \beta_s^2 - \beta_r^2 \tag{2}$$

The up-conversion luminescence spectra of the nanoparticles were measured at room temperature with an Ocean Optics PC2000-CCD spectrometer. Spectral response of the spectrometer was calibrated with Ocean Optics LS-1-CAL-INT calibration source. The excitation source was a HTOE FLMM-0980-711-1300 m fiber-coupled IR laser diode (λ_{exc}=977 nm). There was a long-pass filter (850 nm, Edmunds RG850) between the laser and the sample holder. Sample was inside a capillary tube. Emission was collected at a 90 degrees angle to the excitation. A short-pass filter (850 nm, Edmunds 46386) was used to exclude exciting radiation from the detector. Emission was directed to the detector with an optical fiber (∅ 200 μm). Lenses were used to focus both the excitation and emission radiation. Spectra were collected with the Ocean Optics OOIIrrad software. Laser diode was controlled with a Newport laser diode driver (Model 5060).

Results and discussion

Material impurities

The conventional impurities (NO_3^-, OH^-) in the nanomaterials prepared with the combustion synthesis were observed in the FT-IR spectra (Fig. 1). The amount of these impurities depended on the organic fuel: the highest amount of impurities was observed with urea. As a result of the heat treatment, the organic fuels were decomposed to CO_2, H_2O and NO_x. It is possible that the ZrO_2 nanomaterials contain also carbon residues because the ZrO_2:Yb^{3+},Er^{3+} nanomaterial prepared with the combustion synthesis with urea as the fuel was brown, whereas pure and non-doped ZrO_2 is white. On the other hand, the substitution of Zr^{IV} with Yb^{3+} and Er^{3+} creates oxygen vacancies which may act as color centers. These can absorb in the visible and cause the brownish color. This kind of impurities were not observed in the ZrO_2:Yb^{3+},Er^{3+} nanomaterials prepared with the sol–gel method. This might suggest that there are no or fewer oxygen vacancies or color centers in the products and thus only limited Zr^{IV}/R^{3+} substitution has occurred.

The stretching frequency of the Zr–O bond was observed in the FT-IR spectra at 450 cm^{-1}. This is in agreement with the literature value [12, 16].

Crystal structure and crystallite sizes

The XPD measurements confirmed that the structure of the ZrO_2:Yb^{3+},Er^{3+} nanomaterials was cubic with the space group $Fm\bar{3}m$ (No 225, Z=4) [17] (Fig. 2). The ZrO_2:Yb^{3+},Er^{3+} nanomaterials prepared with the combustion synthesis were pure, whereas small amounts of the monoclinic ($P2_1/a$, No 14, Z=4) [17] and tetragonal ($P4_2/nmc$, No 137, Z=2) [17] ZrO_2 impurity phases were found in the nanomaterials prepared with the sol–gel method.

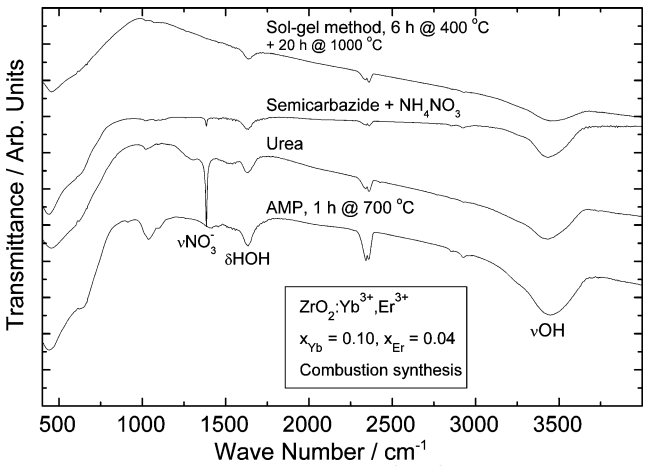

Fig. 1 FT-IR spectra of selected ZrO_2:Yb^{3+},Er^{3+} nanomaterials

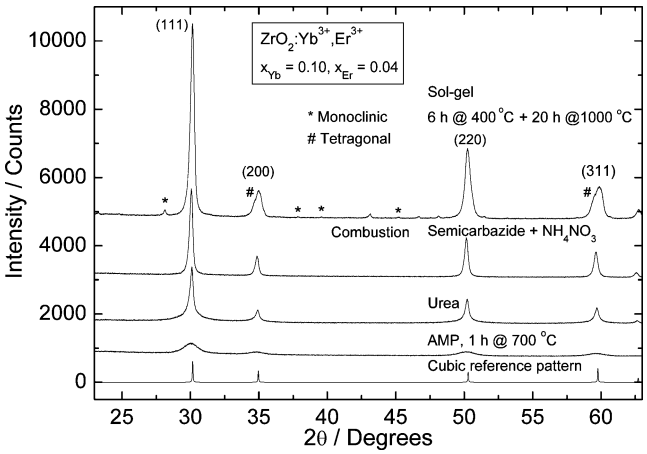

Fig. 2 XPD patterns of selected ZrO_2:Yb^{3+},Er^{3+} nanomaterials

According to the literature [18, 19], the structure of pure ZrO_2 is monoclinic but with small amounts of the trivalent lanthanide doping ions present (*e.g.* Y^{3+}, Eu^{3+}; ionic radii 1.02 and 1.07 Å, respectively [20]) there may exist also tetragonal and cubic phases. In the ZrO_2:Y^{3+},Eu^{3+} system, if the dopant ion level is more than 10% of the zirconium amount [21], there are no more monoclinic or tetragonal phases present, only the cubic one. If the doping level is greater than 57%, one obtains the cubic C-type R_2O_3 phase. Because the ionic radii of Yb^{3+} (0.99) and Er^{3+} (1.00 Å) are closer to that of Zr^{IV} (0.84 Å) than those of Y^{3+} and Eu^{3+}, more Yb^{3+} and Er^{3+} than Y^{3+} and Eu^{3+} can probably be doped in the zirconia host. According to the Vegard's rule, a good solid solubility can occur when the difference in the ionic radii of the host and dopant ions is less than 15%. In addition, the charges should be the same as well as the structures of the pure end member compounds be similar. In the ZrO_2:Yb^{3+},Er^{3+} nanomaterial, the sizes of the ions are close to fulfilling the Vegard's rule. Also the structures of the pure compounds (ZrO_2, C-R_2O_3) are very closely related to the fluorite type structure. Only the charge difference does not favor the solid solubility but this problem is compensated by the charge compensation and the closely related structures. This is valid for the nanomaterials prepared with the combustion synthesis because of the rapid method of synthesis enabling the lanthanide ions to substitute for Zr^{IV}. In contrast, in the nanomaterial prepared with the sol–gel method, the slow reaction rate results in the presence of the monoclinic and/or tetragonal phases. The presence of these zirconium-rich phases is allowed due to the phase segregation. Whether this segregation is partial (with low and high R^{3+} content ZrO_2:Yb^{3+},Er^{3+} phases) or complete (with ZrO_2 and $(Yb,Er)_2O_3$ phases) is not possible to be deduced from the X-ray powder patterns. The total absence of the reflections for the C-R_2O_3 phase suggests the former while the rather strong reflections—so far unknown—may belong to a lanthanide zirconite phase.

The mean crystallite sizes were calculated with the Scherrer equation [15]. The crystallite sizes were 5–30 nm for the nanomaterials prepared with the combustion synthesis and *ca.* 50 nm for those prepared with the sol–gel method. The nanomaterials prepared with semicarbazide and urea were well crystallized compared to the nanomaterial prepared with AMP. The larger crystallite size of the nanomaterials prepared with the sol–gel method is due to the slower crystallization and can be taken as a further indication of the possible phase segregation.

Up-conversion luminescence

The excitation mechanism for the up-conversion luminescence of the Er^{3+} ions under infrared excitation (λ_{exc}= 977 nm) has been well established in the literature [*e.g.* 2, 3]. The first near-infrared (NIR) photon excites the Yb^{3+} ion to the $^2F_{5/2}$ level. From this level the Yb^{3+} ion may relax radiatively back to the ground $^2F_{7/2}$ level. Alternatively, it may transfer the excitation energy to an Er^{3+} ion. The Er^{3+} ion is promoted to the $^4I_{11/2}$ level and further to $^4F_{7/2}$ due to absorption and energy transfer of another NIR photon. From this energy level Er^{3+} decays rapidly and non-radiatively to the $^2H_{11/2}$, $^4S_{3/2}$ or $^4F_{9/2}$ levels. The up-conversion emission is assigned to the following transitions: the red emission in the 650–700 nm region to the $^4F_{9/2}\rightarrow{}^4I_{15/2}$ transitions and the green emission in the 520–580 nm region to the ($^2H_{11/2}$, $^4S_{3/2}$)$\rightarrow{}^4I_{15/2}$ transitions of the Er^{3+} ion.

In the ZrO_2 matrix, the luminescence spectra are composed of broad bands without clear crystal field fine structure. This is due to the several overlapping spectra which in turn are due to the several Er^{3+} (and Yb^{3+}) ion sites with different point symmetries and, even more important, different crystal field strengths. Thus, the broad bands in the luminescence spectra are due to the different charge compensation in the first coordination sphere. Because in the zirconia structure there are no trivalent ion sites, in order to accomplish charge compensation, oxide vacancies (Kröger–Vink notation: $V_O^{\bullet\bullet}$) are formed as a result of the Yb^{3+} and Er^{3+} ions occupying the tetravalent Zr^{IV} site (Yb'_{Zr} or Er'_{Zr}) in the cubic fluorite type structure (Fig. 3).

In the ZrO_2:Y^{3+},Eu^{3+} system there were found at least three different oxide vacancy positions around the R^{3+} ion [21, 22]. Similar behavior is present in the ZrO_2:Yb^{3+},Er^{3+} nanomaterial due to the similar ionic radii of the Y^{3+} and Yb^{3+}.

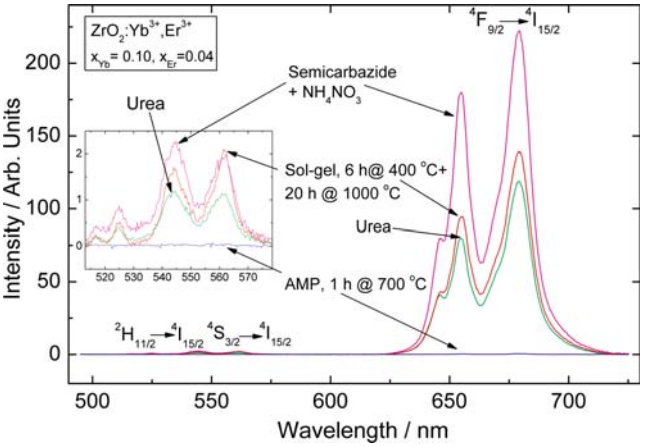

Fig. 4 Up-conversion luminescence spectra of selected ZrO_2:Yb^{3+}, Er^{3+} nanomaterials

In addition, because of the smaller ionic radius of Zr^{IV} compared to those of Yb^{3+} and Er^{3+}, further—but minor—structural distortions around the R^{3+} ions are induced due to the different charge compensation schemes in the outer coordination spheres. These distortions cause the broadening of the individual lines in the luminescence spectra.

In the Kröger–Vink -notation, ● denotes a positive and ′a negative charge relative to the environment of the lattice defect—either an oxygen vacancy or an alivalent R^{3+} ion substituting Z^{IV}, respectively. Owing to the general tendency of defects to form aggregates and because of the electrostatic attraction between the species, $Yb'_{Zr} - V_O^{\bullet\bullet} - Er'_{Zr}$ pairs are formed. These pairs can enhance the absorption efficiency and the energy transfer between Yb^{3+} and Er^{3+} ions though energy migration between Yb^{3+} ions may result, too. The energy migration may cause the excitation energy to reach an impurity and be lost before reaching an Er^{3+} ion.

The most intense up-conversion luminescence was observed from the ZrO_2:Yb^{3+},Er^{3+} nanomaterial prepared with the combustion method with semicarbazide as the organic fuel (Fig. 4). This is due to the structurally pure cubic nanomaterial. The luminescence intensity was very weak from the nanomaterial prepared with the AMP as the fuel. This is due to the small crystallite size (*ca.* 5 nm) and the large surface area of the particles. Large surface area increases the amount of surface defects and the adsorption of impurities (*e.g.* CO_2, H_2O, NO_3^-,) that decrease the luminescence intensity. Although there were considerable amounts of nitrate residues in the nanomaterial prepared with

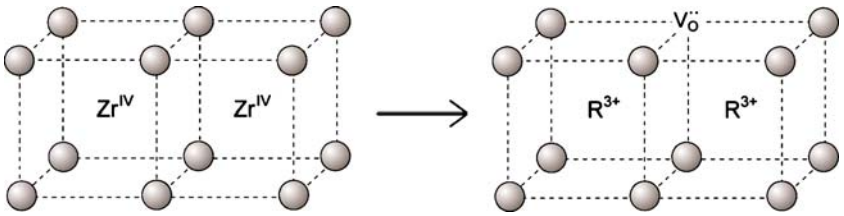

Fig. 3 Structure of the environment of zirconium in ZrO_2 with and without R^{3+} substitution

the urea as the fuel, there were observed rather intense up-conversion luminescence. This is due to the good crystallinity and rather large crystallite size of these nanomaterials.

The crystallite sizes of the ZrO_2:Yb^{3+},Er^{3+} nanomaterials prepared with the sol–gel method were larger when compared to the nanomaterials prepared with the combustion synthesis. Despite this, the luminescence intensity was lower than that of the nanomaterials prepared with the combustion synthesis, except for the nanomaterial prepared with AMP as the fuel. The weak luminescence intensity is probably due to the fact that the sol–gel nanomaterial was a mixture of the cubic, monoclinic and tetragonal forms. This phase separation evidently weakens the luminescence intensity since the optimum concentrations for the R^{3+} ions are lost. Because of the ZrO_2 and R_2O_3 being in separate phases, concentration quenching might occur due to the too high Yb^{3+} and Er^{3+} concentrations in the R_2O_3 phase. Alternatively, if separate low and high R^{3+} content ZrO_2 phases are formed, the R^{3+} concentrations in the latter phase are too high and in the former too low. For this reason, concentration quenching (Er^{3+}) and energy migration (Yb^{3+}) to non-luminescent sites can occur just in a manner similar to R_2O_3. The different surrounding microdomains of the Yb^{3+} and Er^{3+} ions of the nanomaterials prepared with different methods might also affect the absorption efficiency and luminescence intensity.

For the ZrO_2:Yb^{3+},Er^{3+} nanomaterials prepared with the combustion synthesis considerable afterglow was observed. Due to the structural and charge mismatch between the trivalent R^{3+} and Zr^{IV}, there are oxygen vacancies as well as other defects (impurities), (*e.g.* OH^- groups) due to the low temperature preparation method. In the persistent luminescence materials (*e.g.* alkaline earth aluminates MAl_2O_4 and disilicates $M_2MgSi_2O_7$) [23, 24] or photostimulated materials (*e.g.* BaF(Cl,Br)) [25] the energy is stored in these kind of defects. The depths of these traps in the case of the ZrO_2:Yb^{3+},Er^{3+} nanomaterials are compatible with the thermal energy (kT) at room temperature. Thus the thermal feeding from the traps can occur.

Because of the observed afterglow and the up-conversion luminescence in the same nanomaterial, it can be assumed that combining these two phenomena can lead to highly efficient whole-blood immunoassay nanomaterials in the future.

Conclusions

The combustion method was found to be a technique superior to the sol–gel method to prepare the nanocrystalline up-converting ZrO_2:Yb^{3+},Er^{3+} luminescence materials. The structure of the ZrO_2:Yb^{3+},Er^{3+} nanomaterials prepared by the combustion method was cubic, whereas the sol–gel method yielded a mixture of cubic, monoclinic and tetragonal phases. Most of the nanomaterials showed green and red up-conversion luminescence with broad bands. This is due to the multisite positions of the Er^{3+} ion in the ZrO_2 host material. As a result of the structural purity, the highest luminescence intensity was obtained from the nanomaterials prepared with the combustion method.

Although the ZrO_2:Yb^{3+},Er^{3+} nanomaterials were synthesized successfully, the reduction in the crystallite size needs further work for the efficient use in immunoassays. Surface modifications need also to be studied in the future because of the possible applications in aqueous solutions. Also enhancement of the up-conversion luminescence intensity needs further studies because high up-conversion luminescence is needed in homogeneous label technology for immunoassays. Further investigations should also be carried out to optimize the persistent luminescence of the ZrO_2:Yb^{3+},Er^{3+} nanomaterials. This is important for efficient immunoassay nanomaterials where the advantages of both the persistent and up-conversion luminescence are combined.

Acknowledgements Financial supports from the Finnish Funding Agency for Technology and Innovation (Tekes) and the Graduate School of Materials Research (Turku, Finland) for L. Pihlgren and the Graduate School of Chemical Sensors and Microanalytical Systems (Espoo, Finland) for I. Hyppänen are gratefully acknowledged.

References

1. Auzel F (2002) Up-conversion in rare-earth doped systems: past, present and future. Proc. SPIE 4766:179–190
2. Auzel F (2004) Upconversion and anti-Stokes processes with f and d ions in solids. Chem Rev 104:139–173
3. Mita Y (1999) Infrared up-conversion phosphors. In: Shionoya S, Yen WM (eds) Phosphor handbook. CRC Press, Boca Raton, FL, USA, pp 643–650
4. Grubb SG, Bennett KW, Cannon RS, Humer WF (1992) CW room-temperature blue upconversion fibre laser. Electron Lett 28:1243–1244
5. Downing E, Hesselink L, Ralston J, Macfarlane R (1996) A three-color, solid-state, three-dimensional display. Science 273:1185–1189
6. Gutmann R, Ahlers B, Kappe F, Paugstadt R, Franz-Burgholz A (2001) U.S. Patent 6,234,537
7. Misra SN, Gagnani MA, Devi I, Shukla RS (2004) Biological and clinical aspects of lanthanide coordination compounds. Bioinorg Chem Appl 2:155–192
8. Mathis G (1993) Rare-earth cryptates and homogeneous fluoroimmunoassays with human sera. Clin Chem 39:1953–1959
9. Zijlstra WG, Buursma A, Meeuwsen-van der Roest WP (1991) Absorption spectra of human fetal and adult oxyhemoglobin, deoxyhemoglobin, carboxyhemoglobin, and methemoglobin. Clin Chem 37:1633–1638
10. Soini E, Meltola NJ, Soini AE, Soukka J, Soini JT, Hänninen PE (2000) Two-photon fluorescence excitation in detection of biomolecules. Biochem Soc Trans 28:70–74
11. Soukka T, Kuningas K, Rantanen T, Haaslahti V, Lövgren T (2005) Photochemical characterization of up-converting inor-

ganic lanthanide phosphors as potential labels. J Fluoresc 15:513–528
12. Patra A, Friend CS, Kapoor R, Prasad PN (2002) Up-conversion in Er^{3+}:ZrO_2 nanocrystals. J Phys Chem B 106:1909–1912
13. Vetrone F, Boyer J-C, Capobianco JA, Speghini A, Bettinelli M (2004) Significance of Yb^{3+} concentration on the upconversion mechanisms in codoped Y_2O_3:Er^{3+},Yb^{3+} nanocrystals. J Appl Phys 96:661–667
14. Díaz-Torres LA, De la Rosa-Cruz E, Salas P, Angeles-Chavez C (2004) Concentration enhanced red upconversion in nanocrystalline ZrO_2:Er under IR excitation. J Phys D Appl Phys 37:2489–2495
15. Klug HP, Alexander LE (1959) X-ray powder diffraction procedures. Wiley, New York, p 491
16. De la Rosa E, Diaz-Torres LA, Salas P, Rodriguez RA (2005) Visible light emission under UV and IR excitation of rare earth doped ZrO_2 nanophosphors. Opt Mater 27:1320–1325
17. PCPDFWIN v. 1.30, 1997, Powder Diffraction File, International Centre for Diffraction Data, entries 27-0997 (cubic), 37-1484 (monoclinic) and 42-1164 (tetragonal ZrO_2)
18. Gupta TK, Bechtold JH, Kuznicki RC, Cadoff LH, Rossing BR (1977) Stabilization of tetragonal phase in polycrystalline zirconia. J Mater Sci 12:2421–2426
19. Ho S-M (1982) On the structural chemistry of zirconium oxide. Mater Sci Eng 54:23–29
20. Shannon RD (1976) Revised effective ionic radii and systematic studies of interatomic distances in halides and chalcogenides. Acta Cryst A 32:751–752
21. Dexpert-Ghys J, Faucher M, Caro P (1984) Site selective spectroscopy and structural analysis of yttria-doped zirconias. J Solid State Chem 54:179–192
22. Tuilier MH, Dexpert-Ghys J, Dexpert H, Lagarde P (1987) X-ray absorption study of the ZrO_2–Y_2O_3 system. J Solid State Chem 69:153–161
23. Aitasalo T, Hölsä J, Jungner H, Lastusaari M, Niittykoski J (2006) Thermoluminescence study of persistent luminescence materials: Eu^{2+}- and R^{3+}-doped calcium aluminates, $CaAl_2O_4$:Eu^{2+},R^{3+}. J Phys Chem B 110:4589–4598
24. Aitasalo T, Hölsä J, Laamanen T, Lastusaari M, Lehto L, Niittykoski J, Pellé F (2005) Luminescence properties of Eu^{2+} doped dibarium magnesium disilicate, $Ba_2MgSi_2O_7$:Eu^{2+}. Ceram-Silik 49:58–62
25. Schweizer S (2001) Physics and current understanding of X-ray storage phosphors. Phys Status Solidi A 187:335–393